Computed Tomography (CT)

Roger Fulton

- Faculty of Medicine and Health, University of Sydney, Australia.
- Department of Medical Physics, Westmead Hospital, Sydney, Australia.

roger.fulton@sydney.edu.au
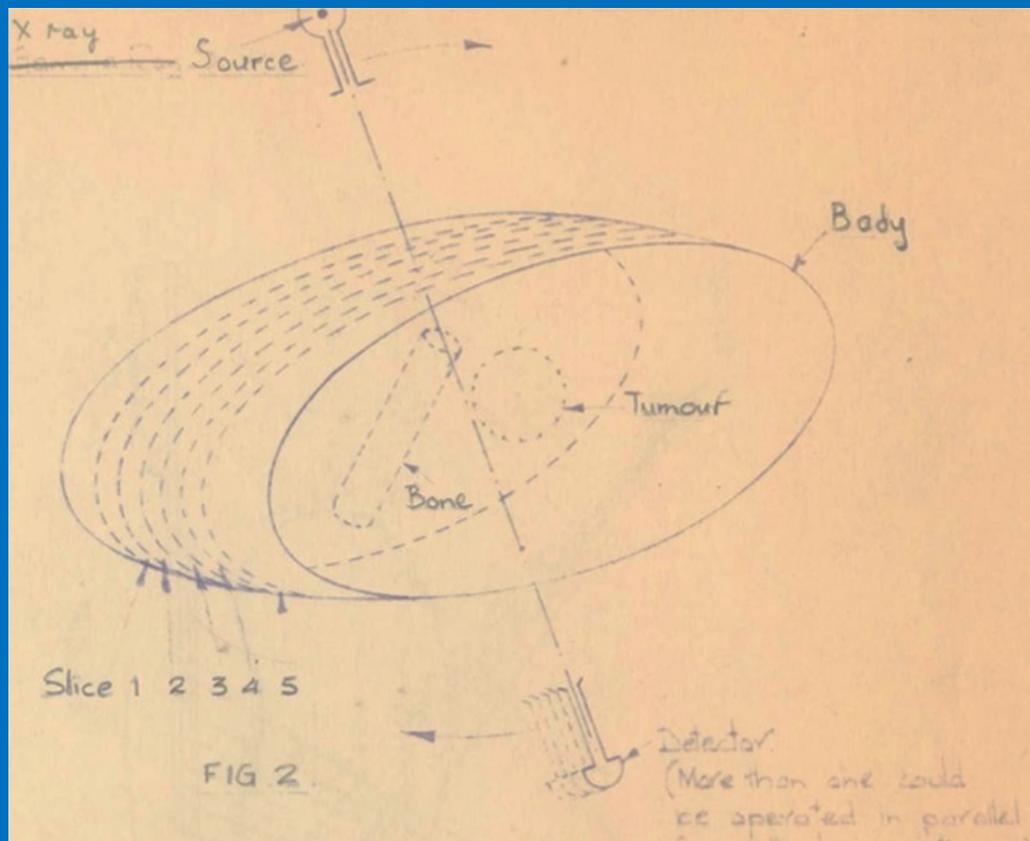
THE UNIVERSITY OF
SYDNEY

Outline

- CT Fundamentals

- Data acquisition and reconstruction

- Image quality

- Radiation dose

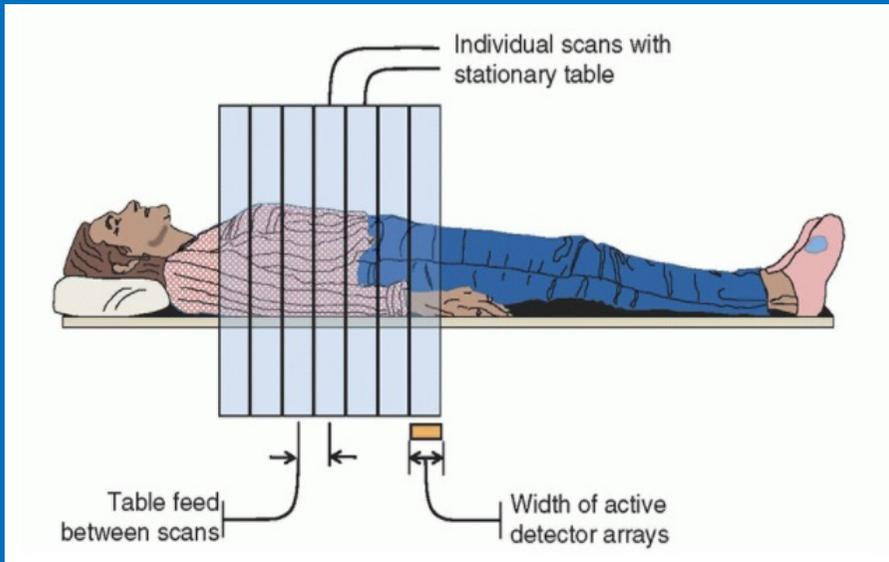- Photon counting CT

Fundamentals

What is CT?

From "An improved form of x-radiography", G. Hounsfield, Research Laboratories of Electric and Musical Industries, Ltd., Middlesex, 1967, in Schulz R, et al, Journal of Medical Imaging, 8(5), 2021, doi: 10.1117/1.JMI.8.5.052110.

CT scanning
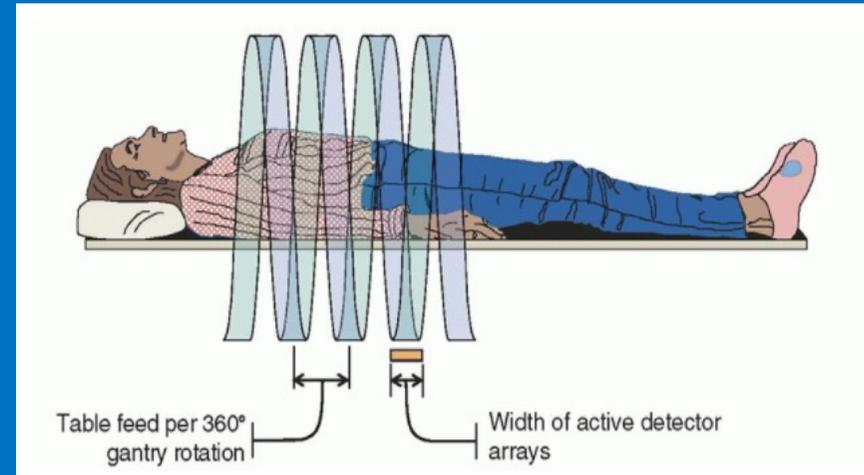
- Rotate an x-ray tube and detectors around a body part

- Measured the intensity of the transmitted beam with the detector array.

Detectors

X-ray tube
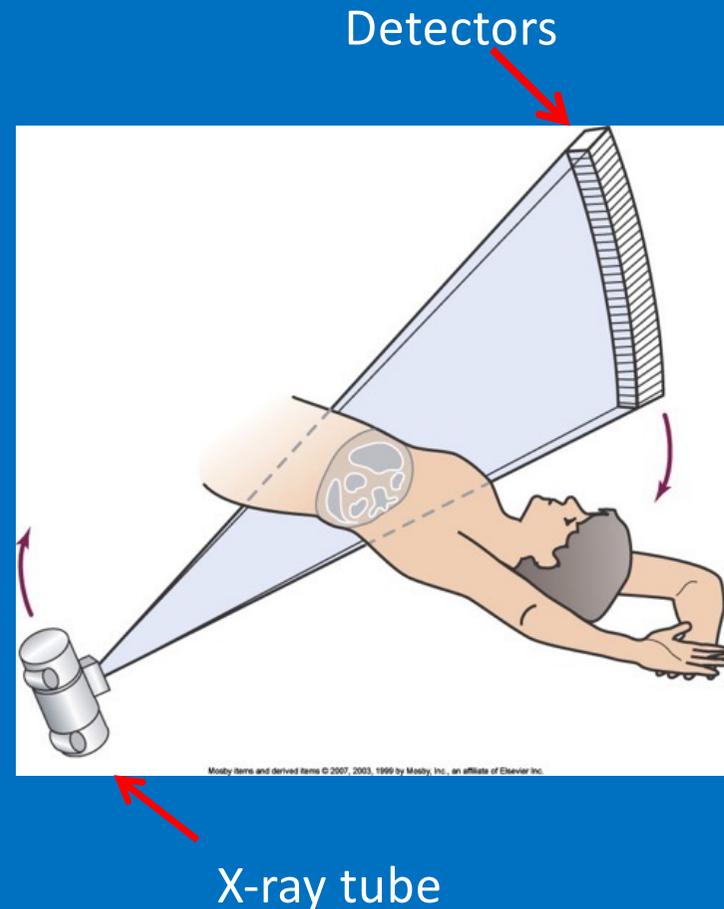
Acquisition modes

Axial

Spiral (Helical)

Bushberg, J. T. et al., (2021). *The essential physics of medical imaging* (Fourth edition.). Wolters Kluwer.

Pitch

$$\text{Pitch} = \frac{\text{table travel / rotation}}{\text{X-ray beam width}}$$

T = 80

z-axis

X = 40

Pitch = 2

T = 40

z-axis

Pitch = 1

IAEA

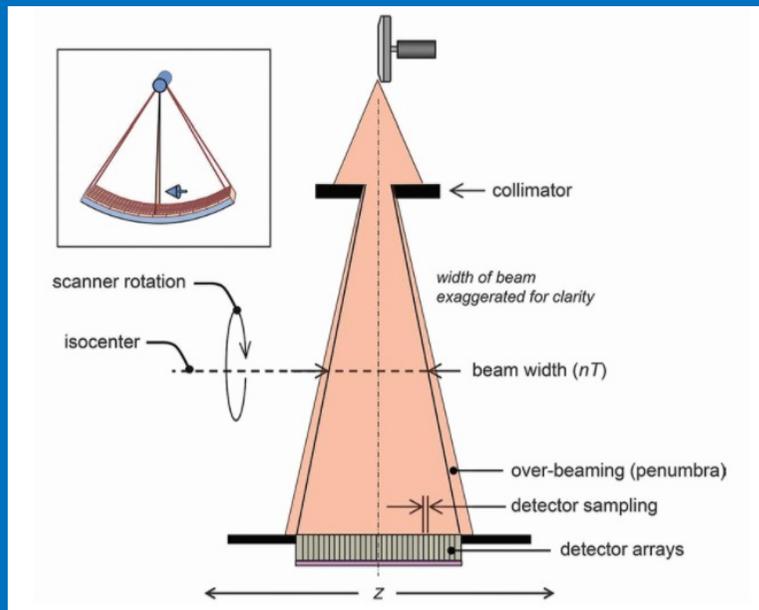Diagnostic Radiology Physics: a Handbook for Teachers and Students – chapter 11, 96
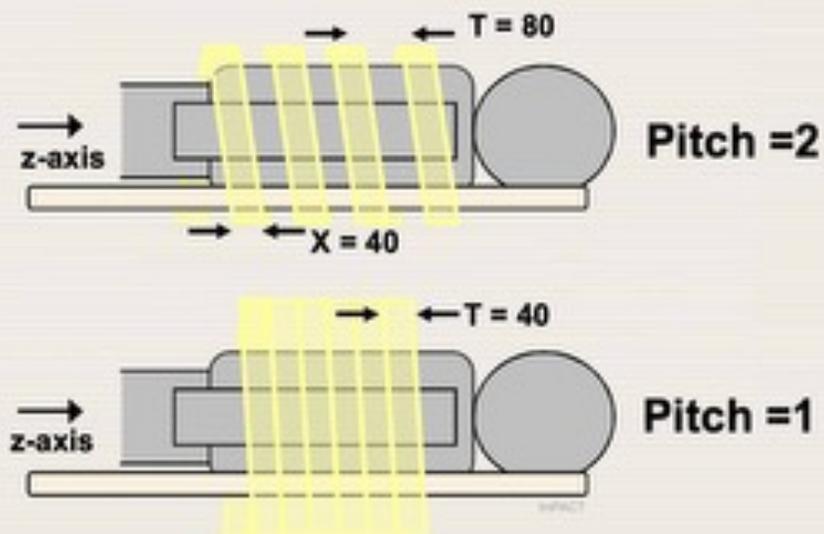
T = bed travel per rotation
X = beam width

Multislice CT
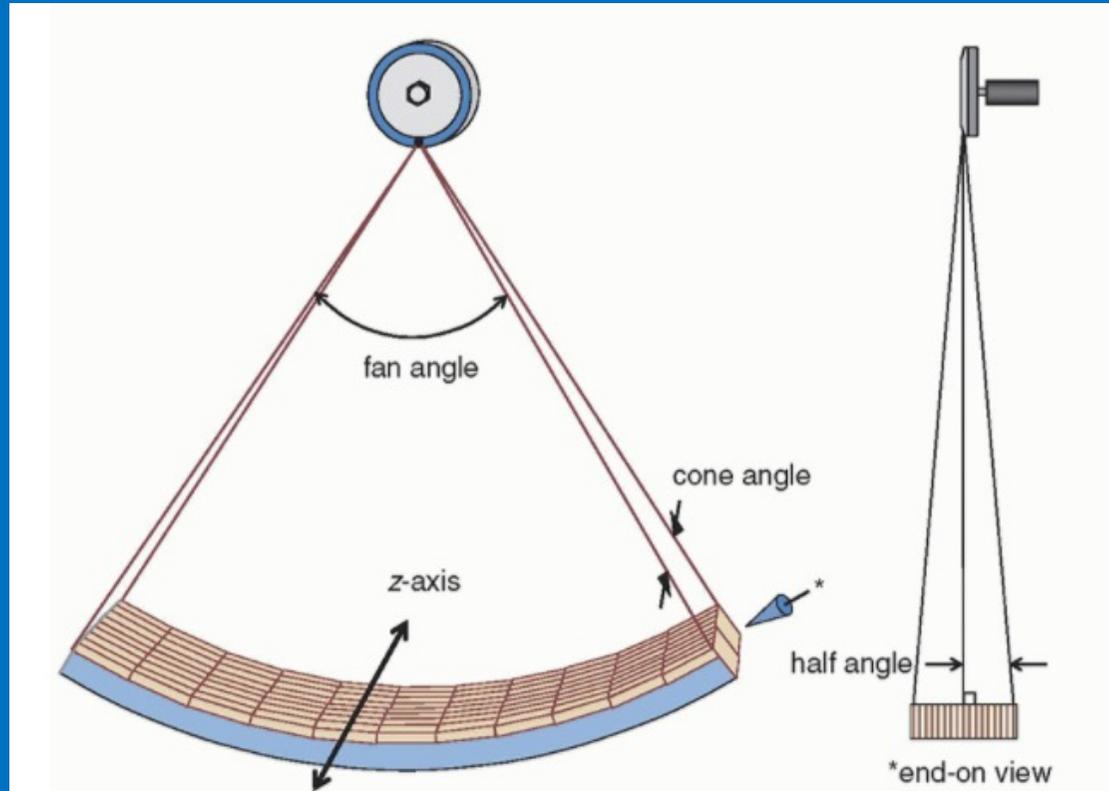
Bushberg, J. T. et al., (2021). *The essential physics of medical imaging* (Fourth edition.). Wolters Kluwer.

Beam Collimation

Bushberg, J. T. et al., (2021). *The essential physics of medical imaging* (Fourth edition.). Wolters Kluwer.
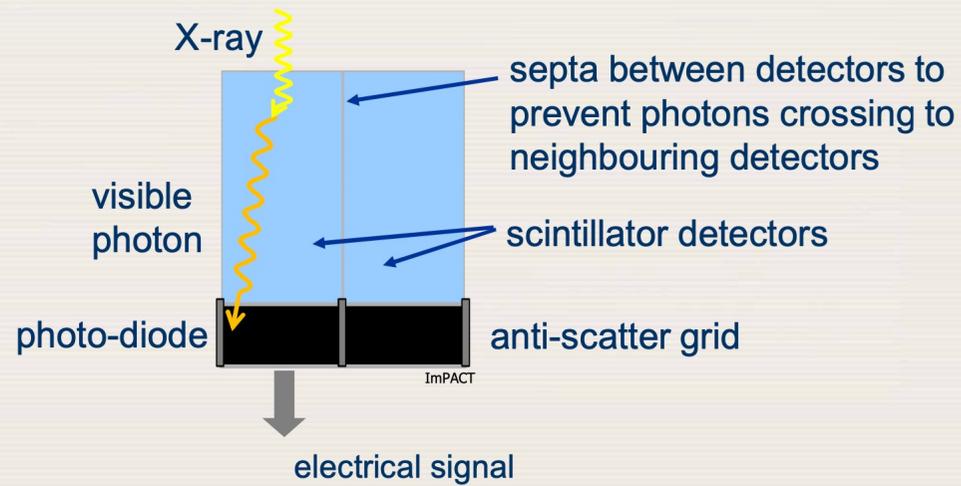
- Controls the beam width and reduces scattered radiation.

- In single slice CT (SSCT), collimation was adjusted to set the slice thickness.

- In multislice CT (MSCT) it is adjusted to make the beam width cover the desired portion of the multirow detector array, and slice thickness is determined by beam width and the detector array configuration.

Data acquisition and reconstruction

Scintillation Detector

X-ray

septa between detectors to prevent photons crossing to neighbouring detectors

visible photon

scintillator detectors

photo-diode

anti-scatter grid

ImPACT

electrical signal

IAEA

Diagnostic Radiology Physics: a Handbook for Teachers and Students – chapter 11, 40

The Radon Transform

The integral of a 2D image along a line through the body.

$$\int_L \mu(x)\,dx \quad \cong \quad \sum_{i=1}^{N} \mu_i \Delta x$$

$$S_j = S_r e^{-\sum_{i=1}^{N} \mu_i \Delta x}$$

$$\ln\left(\frac{S_r}{S_j}\right) = \sum_{i=1}^{N} \mu_i \Delta x$$
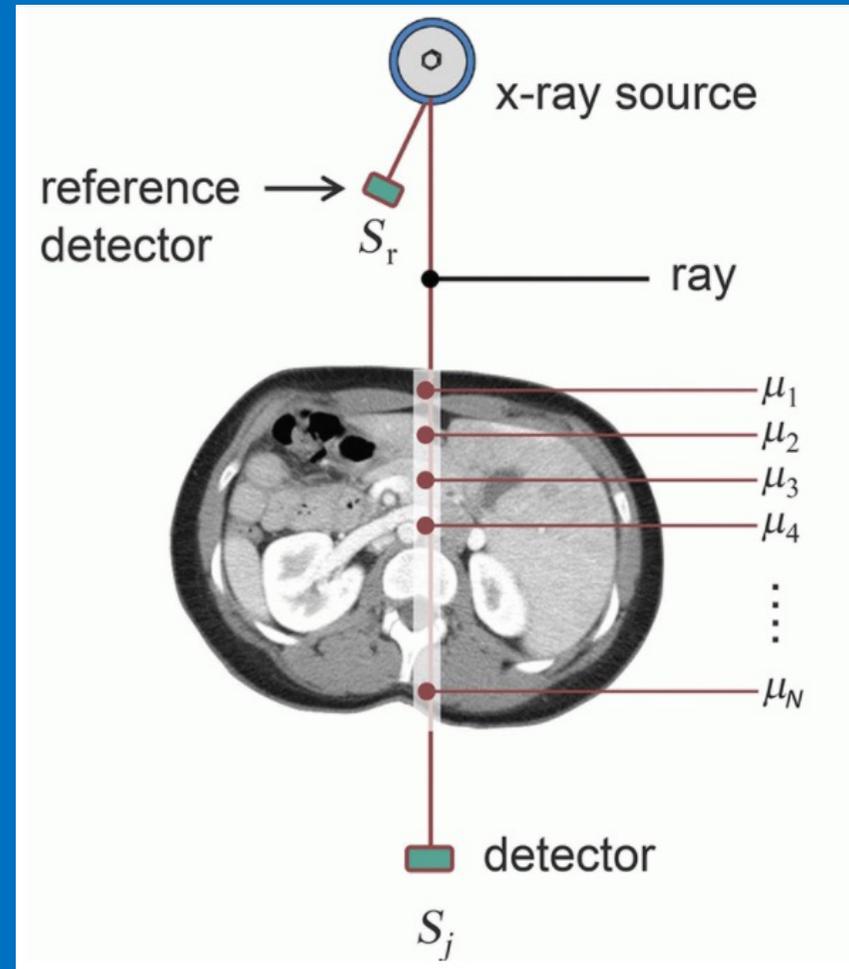
Filtered back projection (FBP)

PET
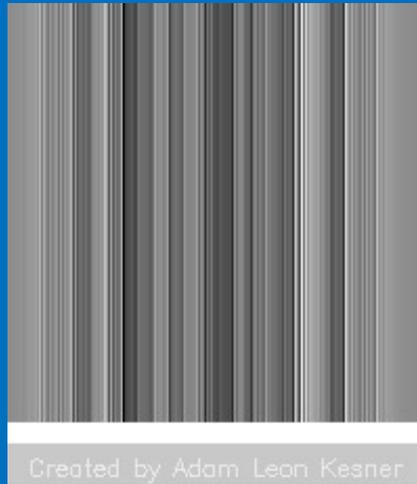
CT
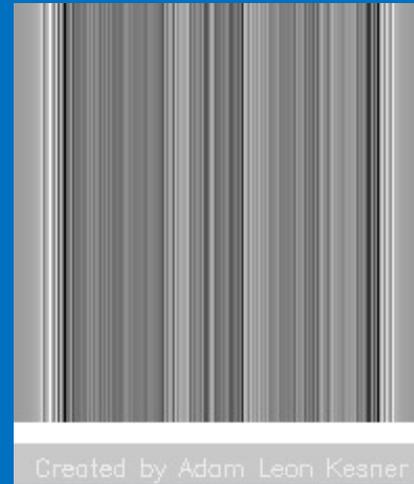
Statistical Image Reconstruction

FBP
at 100% dose

Iterative reconstruction
at 40% dose

Images courtesy of Siemens Healthineers, Forcheim, Germany

Speed vs Image Quality and Dose

FBP
(seconds)

ASIR
(a bit longer)

Model based image
reconstruction (MBIR)
(an hour or more)

increasing reconstruction time →

increasing image quality (at matched dose) →

decreasing dose (at matched SNR) →

Deep Learning Tomographic Reconstruction

- DL has been used in all imaging modalities and, just like MBIR, it is very good at reducing noise or radiation dose while preserving high frequency details
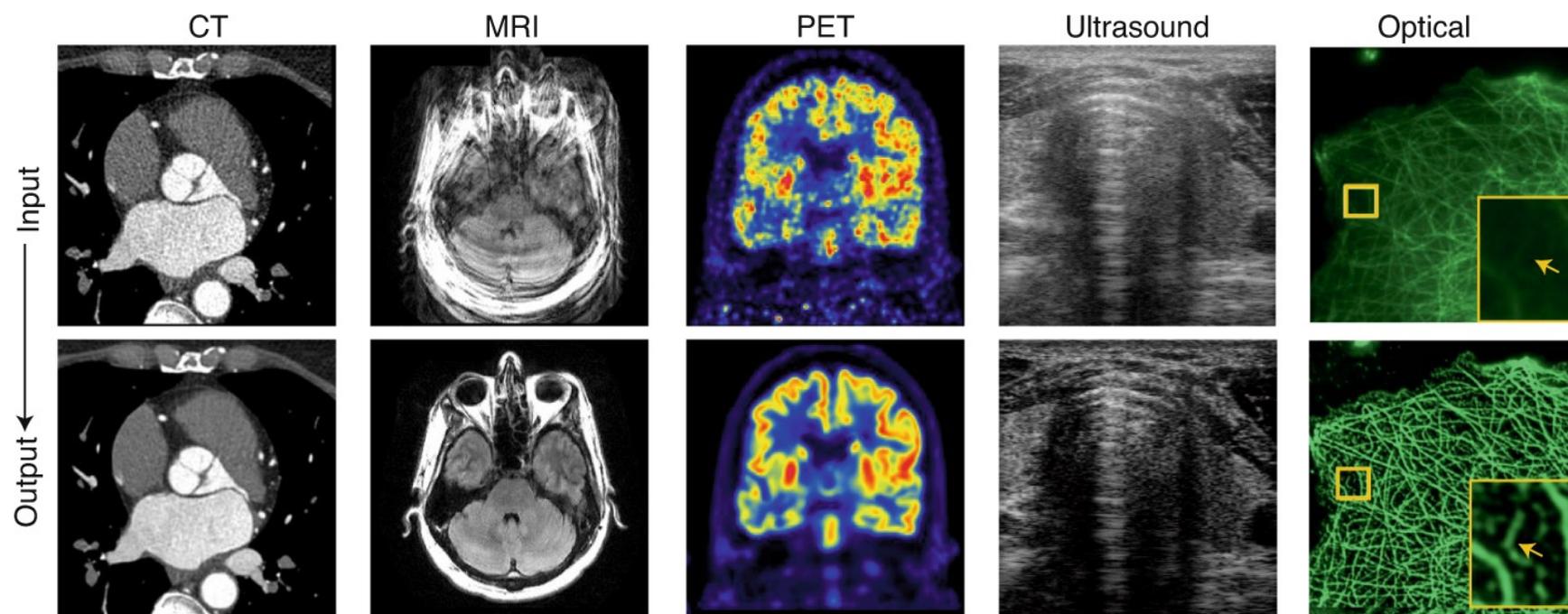
Wang, G. et al. Deep learning for tomographic image reconstruction. *Nat Mach Intell* 2: 737–748 (2020) https://doi.org/10.1038/s42256-020-00273-z

CT image quality

In-plane spatial resolution

Catphan 600 high resolution insert.

- Bar patterns of varying separation in a uniform background material.

- Two impulse sources (tungsten carbide beads for estimating the point spread function (PSF).
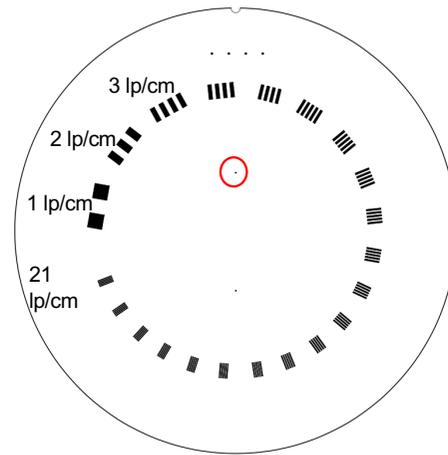
Schematic
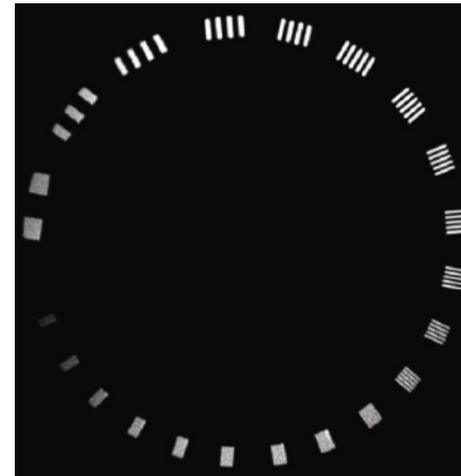
Reconstructed image

Modulation Transfer Function (MTF)

- A plot of spatial frequency recovery (or preservation) vs spatial frequency.

- MTF can be used to determine a scanner's resolution capability, or to compare the performance of different CT systems.

Modulation transfer function (MTF) curve
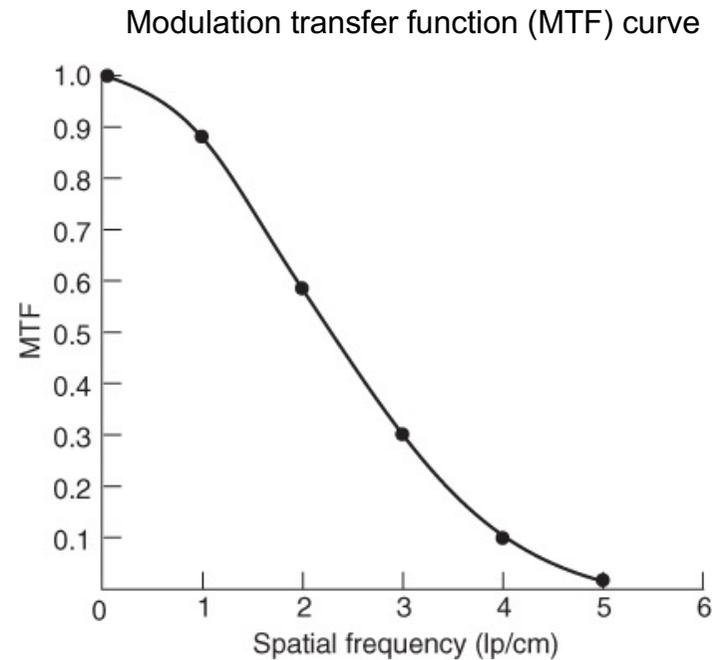
Factors Affecting In-Plane Spatial Resolution

- Focal spot size and shape
- Detector element size
- Sampling
- Reconstructed matrix size
- Reconstruction algorithm

Flying Focal Spot

Deflecting the focal spot in the X-Y and/or Z plane between adjacent detector read–outs.

Doubles the in-plane or cross-plane sampling density.

Can improve resolution and reduce aliasing artifacts.

❑ Dynamic or flying focal spot
- Focal spot position on anode is rapidly oscillated during gantry rotation, doubling the number of projections
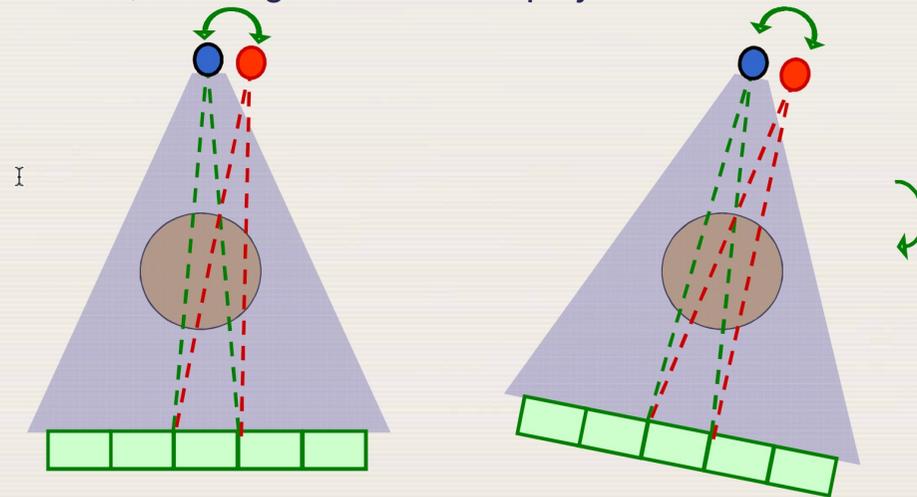
Schematic view of dynamic focal spot – X-Y plane

IAEA

Low-Contrast Detectability (LCD)

- Measured with phantoms that contain low-contrast objects of different sizes, at three different contrast levels, 0.3%, 0.5%, 1%.

- Designed such that 1% contrast equates to a difference of 10 HU.

- The CT scanner's low-contrast detectability (LCD) is determined by the smallest object that can be visualized at a given contrast level and dose.
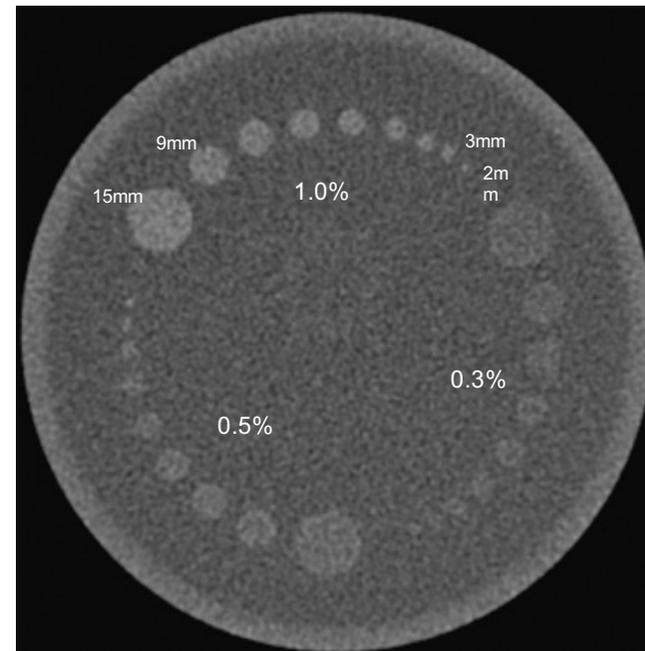
The low-contrast portion of the Catphan phantom.

Seeram, E. (2008). Computed Tomography: Physical Principles, Clinical Applications, and Quality Control. In *Computed Tomography*. Elsevier.

Factors That Affect Low-Contrast Detectability

- Object size
- Contrast (intensity difference) to the background
- Noise
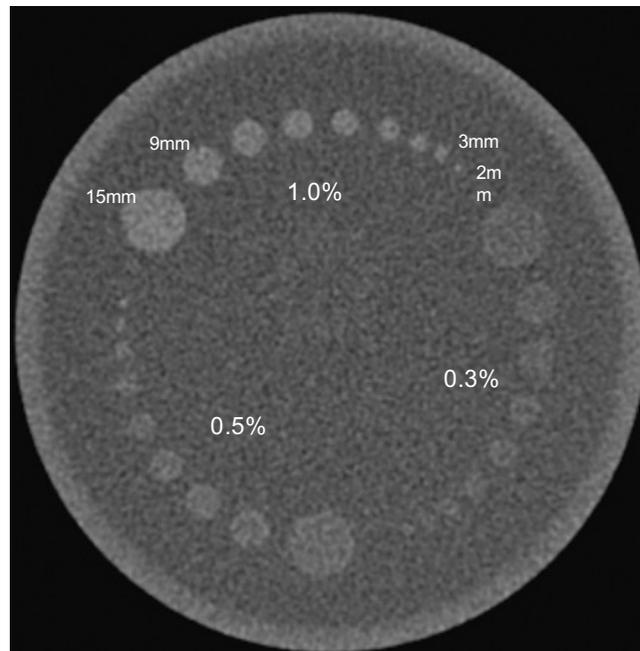
The low-contrast portion of the Catphan phantom.

Seeram, E. (2008). Computed Tomography: Physical Principles, Clinical Applications, and Quality Control. In *Computed Tomography*. Elsevier.

Factors influencing noise and hence low-contrast detectability

- Increasing **tube curren**t reduces noise, but increases patient dose and the tube heat loading.

- \Increasing **tube voltage** improves photon statistics and thereby reduces noise, but reduces the proportion of low-energy photons necessary to visualise low contrast objects.

- Increasing **slice thickness** reduces noise (since more photons contribute to the slice) but the partial volume effect reduces the visibility of small objects.

- Increasing **scan duration** reduces noise, but increases radiation dose..

- Reconstruction algorithm.

CT Radiation Dose

Phantoms for CT Dose Measurement

- To standardize measurement of dose, two cylindrical BRH* phantoms are used
  - 16 cm diameter simulates the patient's head
  - 32 cm diameter simulates the patient's body
- A pencil ionization chamber measures the amount of charge generated.

*Bureau of Radiological Health

100 mm pencil chamber

PMMA plug

32 cm body PMMA phantom

peripheral hole

center hole

16 cm head PMMA phantom
also, pediatric body phantom

Pencil chamber

PMMA phantom

primary x-ray beam

scattered x-rays
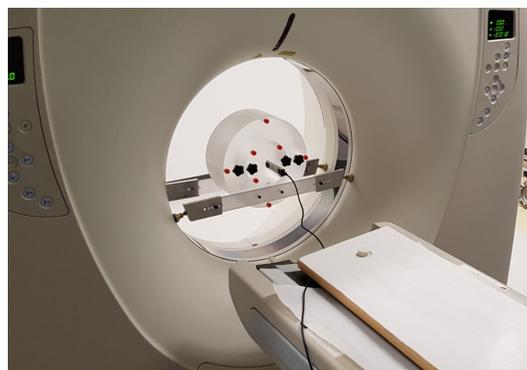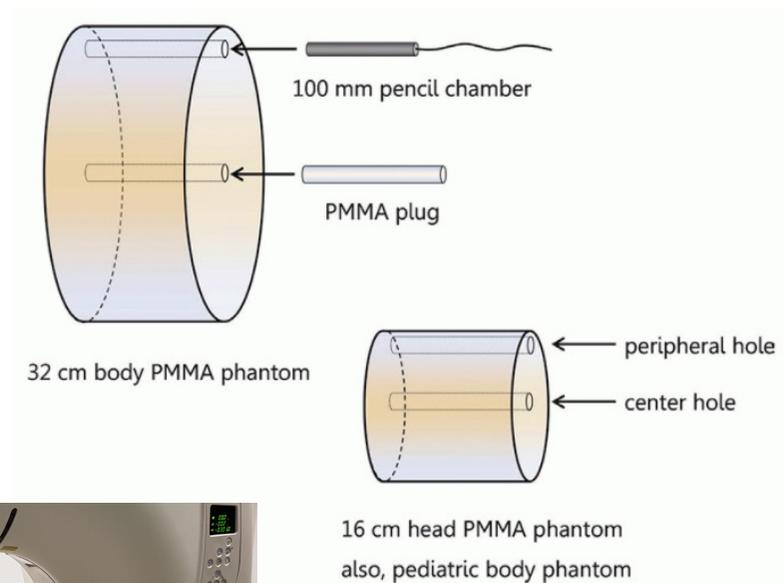
100 mm long
pencil chamber
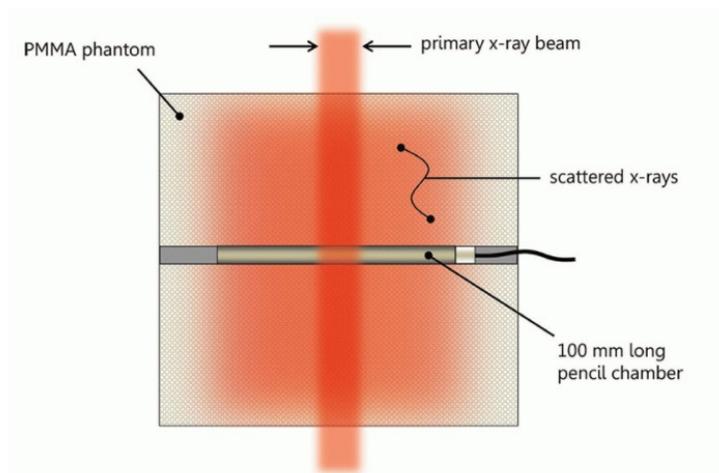
<10% of the dose at the center of the phantom is due to the primary beam, the remaining 90% being due to scatter.

CTDI$_{100}$

Defined as

$$CTDI_{100} = \frac{1}{nT} \int_{-50mm}^{+50mm} D(z)dz$$

where D(z) is the dose distribution along the z axis from a single circular rotation of the scanner with a nominal collimated beam width of nT. It is a measurement of the primary and scattered radiation measured over a 100 mm length, from -50 to +50 mm, where the centre of the x-ray beam is positioned at Z =0, divided by the nominal beam width.

- Measurements are made at both the centre and periphery.

- Units: mGy.

AAPM Report No. 96, 2008

CTDI$_W$

Since CTDI$_{100}$ varies with depth, another index has been developed to provide a better average measure of dose within the X-Y plane - CTDI$_w$. It combines the centre and peripheral CTDI$_{100}$ measurements using a 1/3 and 2/3 weighting scheme provides a good estimate of the average dose to the phantom at the central CT slice. This average is the weighted CDTI, CTDI$_W$.

$$CTDI_W = \frac{1}{3}CTDI_{100,centre} + \frac{2}{3}CTDI_{100,periphery}$$

- Units mGy.

- Gives a more realistic dose estimate than the CTDI$_{100.}$

CTDI$_W$ dependence on helical pitch

CT dose is inversely proportional to the helical pitch used, i.e.

$$\text{dose} \propto \frac{1}{\text{pitch}}$$

To account for this dependency of dose on pitch, the CTDI$_W$ is converted to the volume CTDI (CTDI$_{vol}$) using

$$CTDI_{vol} = \frac{CTDI_W}{\text{pitch}}$$

Dose Length Product (DLP)

The dose length product (DLP) is the product of the CTDI$_{vol}$ and the scan length, L, of the CT scan along the Z axis of the patient.

$$DLP = CTDI_{vol} \times L$$

- Units mGy-cm
- Better related to the patient's radiation risk than CTDI$_{vol}$.

Effective Dose

- If the DLP is known, effective dose can also be obtained by multiplying the DLP with a previously-established k-value for the body part imaged, with very comparable results

$$E = k \times DLP$$

- Units: mSv
- k-values (mSv/mGy-cm): Head (0.0021), Chest (0.017), Abdomen (0.015), Abdomen-pelvis (0.015), Pelvis (0.015).

Longitudinal (z) Tube Current Modulation

- Adjusts the tube current as patient attenuation changes in the longitudinal (z) direction.
- Maintains a uniform noise level despite differences in thickness and attenuation of body parts examined.
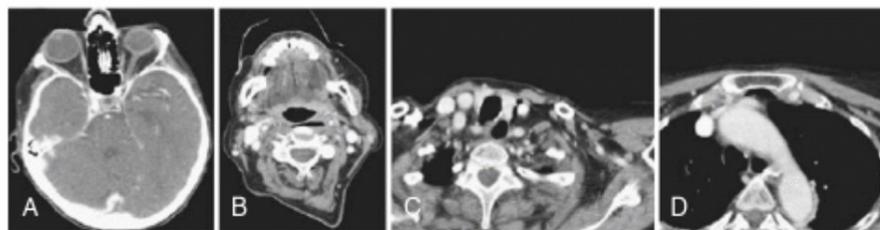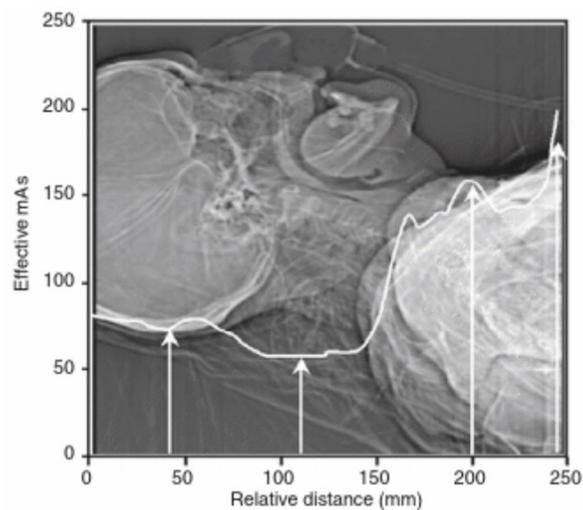
| 75 mAs | 58 mAs | 160 mAs | 200 mAs |

Angular (X-Y axis) Tube Current Modulation

- Adjusts the tube current as the x-ray tube rotates around the patient to compensate for attenuation changes with view angle.
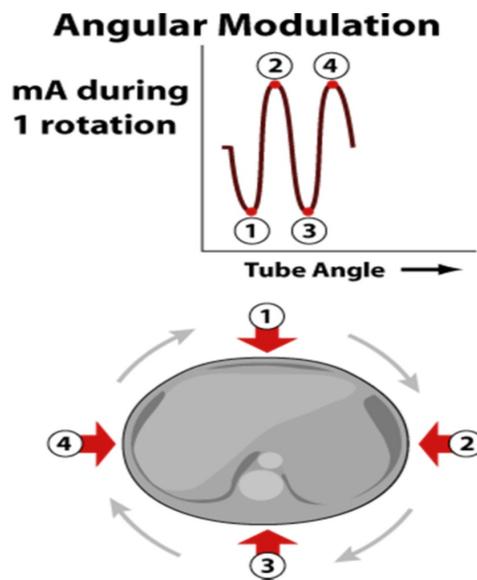
Dose Relationships

$$Dose \propto mAs$$

$$Noise \propto \frac{1}{\sqrt{mAs}}$$

$$Noise \propto \frac{1}{\sqrt{Dose}}$$

$$Dose \propto \frac{1}{\text{pitch}}$$

$$Dose \propto kVp^2$$

$$Dose \propto \text{Beam width}$$

Photon counting CT

CT Detector Types

Energy Integrating Detector — Dual Layer Detector — Direct Conversion Detector

X-Ray Photons

Scintillator / Photo Diode / Integrating ASIC → Integrated Energy (white light intensities)

Low density Scintillator / High density Scintillator / Photo Diode / Integrating ASIC → Integrated Two Energies (low and high energy intensities)

Direct Conversion Material / Counting ASIC → Spectral Profile (Discrimination and count)

Shefer, E., Altman, A., Behling, R., et al. (2013). *Current Radiology Reports*, *1*, 76-91.)

The Photon Counting Detector

Figure 1: Diagrams show detector types. *A*, In conventional energy-integrating detector, an incident x-ray photon is converted into a shower of visible light photons in a scintillator. Visible light hits an underlying light sensor, where it generates positive and negative electrical charges. *B*, In photon-counting detector, the x-ray photon is absorbed in a semiconductor material, where it generates positive and negative charges. Under the influence of a strong electric field, the positive and negative charges are pulled in opposite directions, generating an electrical signal.

Willemink et al, Radiology 289 (2), 2018,
10.1148/radiol.2018172656

- In photon-counting detectors (PCDs) each individual photon that hits the detector element generates an electrical pulse with a height proportional to the energy deposited by the photon.

- The electronics system of the detector counts the number of pulses with heights that exceed preset threshold levels.

Principle

Figure 2: Diagram illustrates operating principle of a photon-counting detector. Each registered photon gives rise to an electrical pulse in the detector readout electronics, with the height of each pulse proportional to the individual photon energy. The detector counts the number of pulses with 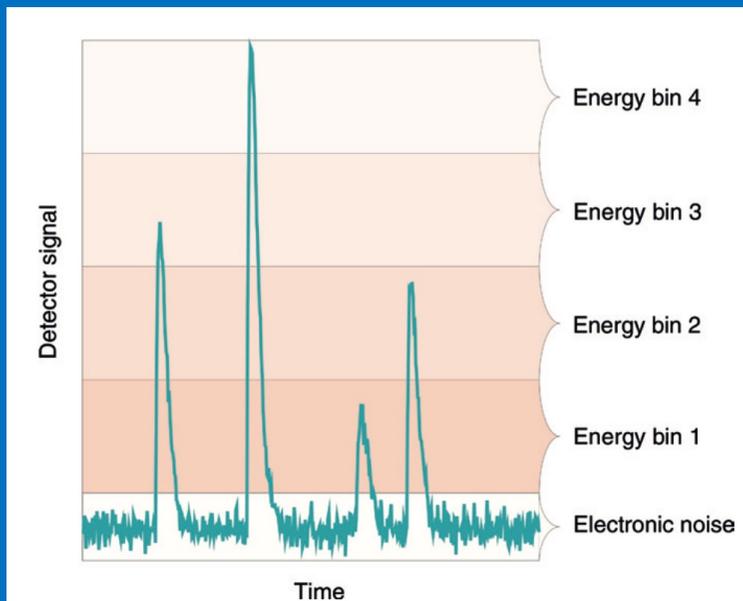a height larger than a preset threshold, thereby eliminating electronic noise. By setting more than one threshold, the registered photons can be sorted into several energy bins on the basis of their energy range.

- Thresholds are set at levels that are higher than the electronic noise level but lower than pulses generated by incoming photons.

- By comparing every pulse to threshold levels, the detector can sort the incoming photons into a number of energy bins (typically two to eight), depending on their energy.

- Electronic noise is effectively excluded

Low energy benefit

- In an EID, high-energy photons contribute relatively more to the total signal than low-energy photons, but the tissue contrast is low at high energies.

- This results in low contrast to noise ratio (CNR).

- A PCD is able to optimise CNR by assigning the largest weight to photons with low energies, for which the contrast (difference in attenuation coefficient) between tissues is the highest.
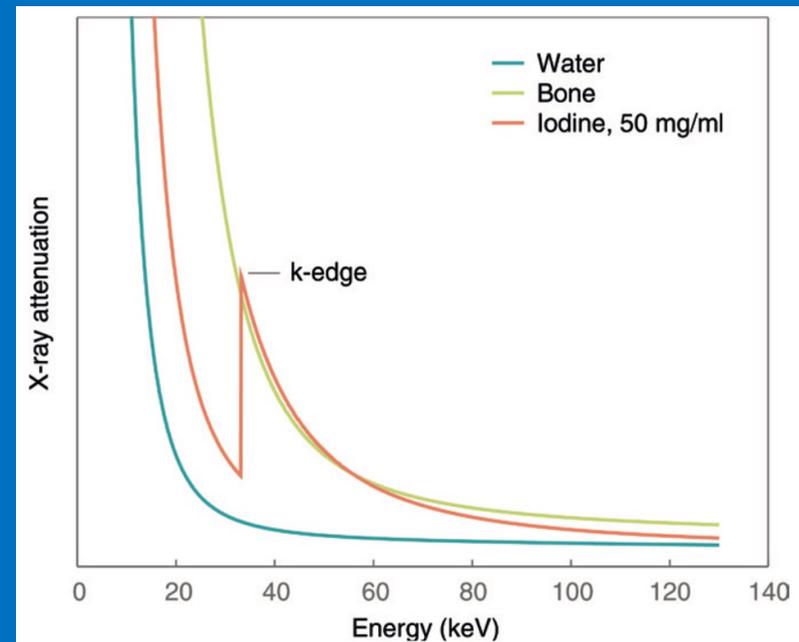
Figure 7: Graph shows attenuation coefficient as a function of energy for water, bone, and iodinated contrast agent (50 mg iodine per milliliter). The difference between the attenuation coefficients for different materials is largest for low energies. A heavy element such as iodine has a k-edge in the diagnostic energy range and can therefore be uniquely identified with an energy-resolving measurement.

Willemink et al, Radiology 289 (2), 2018, 10.1148/radiol.2018172656

Spatial resolution benefit

- The spatial resolution achievable with any CT detector is primarily determined by its detector element size, which is close to 1 x 1 mm^2 for current systems.

- EID detector elements must be separated from each other by thin, reflective septa to prevent light entering adjacent scintillators.

- PCDs use direct conversion detectors (no septa) that can be manufactured with smaller detector elements (0.11x0.11 to 0.5x0.5 mm).

Material decomposition example (in vivo)

A Grayscale image   **B** Multimaterial map

- Iodine
- Gadolinium
- Bismuth

C Iodine map   **D** Gd map   **E** Bi map   **F** Calcium map

Figure 13: Example of in vivo multi k-edge material imaging of canine performed with photon-counting detector (PCD) CT. *A*, Grayscale PCD image reconstructed from all photons detected, regardless of their detected energy, at level of left pelvis demonstrates the dense contrast material in calibration vials, abdominal aorta, and kidney. No differentiation is possible between the different contrast agents with single-energy CT. *B*, PCD multimaterial map enables differentiation between iodine, gadolinium, and bismuth contrast agents. *C*, Iodine, *D*, gadolinium (*Gd*), *E*, bismuth (*Bi*), and, *F*, calcium material maps reveal calibration vials containing different contrast agents, with arterial corticomedullary iodine enhancement and venous nephrogenic and/or excretory enhancement within kidney. (Reprinted, with permission, from reference 49.)

Radiation Dose and Image Quality with PCDs

- Image noise levels lower at the same level of x-ray exposure compared with conventional CT scanners.

- Dose reduction of about 30% (first studies).

- Improved contrast-to-noise ratio (CNR).

- Improved spatial resolution compared with conventional EIDs.

PCD Spatial Resolution
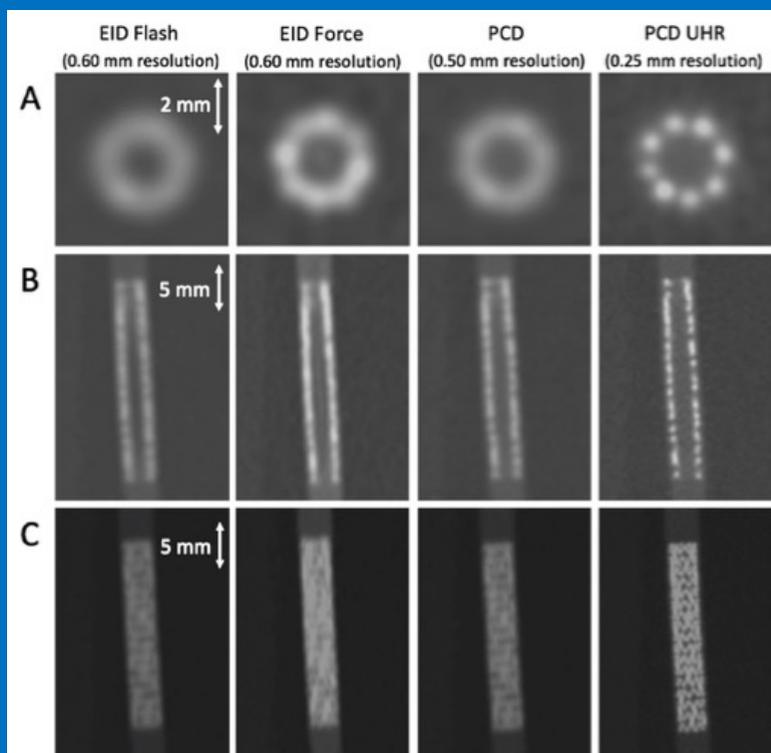
Figure 17: High-spatial-resolution dual-energy photon-counting detector (PCD) improves resolution and reduces blooming. A, Axial, B, coronal, and, C, coronal maximum intensity projections of scans of coronary stent (Synergy Monorail; Boston Scientific, Marlborough, Mass) made of a platinum chromium alloy, with nominal diameter of 2.75 mm, inside a coronary artery phantom consisting of plastic tubes filled with iodine-based contrast material diluted to approximate clinical concentrations (450 HU at 120 kV). Dual-energy energy-integrating detector (EID) images were acquired by using second- and third-generation dual-source CT systems (Somatom Flash and Somatom Force; Siemens Healthcare, Forchheim, Germany) at 0.60-mm isotropic voxel size. Radiation dose–matched PCD images were obtained with a prototype PCD system (Siemens Healthcare) at standard resolution (macro mode) and high resolution (UHR) (sharp mode). All images were reconstructed by using optimized convolution kernels and filtered backprojection algorithm. (Images from National Institutes of Health [69].)

First clinical PCT scanner (2021)

- NAEOTOM Alpha
  (Siemens Healthineers)

The Future

"In a few years from now every CT will be a photon counting CT". (Thomas Flohr, Siemens Healthineers, 2022).

https://www.siemens-healthineers.com/en-au/computed-tomography/ct-technologies-and-innovations/photon-counting-ct

Other companies developing PCCT systems:
- Samsung Healthcare
- Canon Medical Systems
- GE Healthcare
- Philips Healthcare

Photon-Counting CT: High Resolution, Less Radiation: Emerging Health Technologies, Canadian Agency for Drugs and Technologies in Health; 2024 Feb.

References

- Seeram E, Computed tomography : physical principles, clinical applications, and quality control, Elsevier 4th ed. 2016

- Bushberg J, The essential physics of medical imaging, Wolters Kluwer 4th ed. 2020.

- ImPACT presentations, http://www.impactscan.org/presentations.htm

- Diagnostic Radiology Physics Handbook, http://www-naweb.iaea.org/nahu/DMRP/DiagnosticRadiologyPhysicsHandbook.html

- Goldman L, Principles of CT: multislice CT, *J. Nucl. Med. Technol.* 2008 36:57-68

- Willemink M.J. et al., Photon-counting CT: Technical Principles and Clinical Prospects, *Radiology* 2018: 289:293-312. https://doi.org/10.1148/radiol.2018172656

- https://www.siemens-healthineers.com/en-au/computed-tomography/technologies-and-innovations/photon-counting-ct